C3.4 Heaving and Pitching Airfoil in Wake

1. Code description

XFlow is a high-order discontinuous Galerkin (DG) finite element solver written in ANSI C, intended to be run on Linux-type platforms. Relevant supported equation sets include compressible Euler, Navier-Stokes, and RANS with the Spalart-Allmaras model. High-order is achieved compactly within elements using various high-order bases on triangles, tetrahedra, quadrilaterals, and hexahedra. Parallel runs are supported using domain partitioning and MPI communication. Visual post-processing is performed with an in-house plotter. Output-based adaptivity is available using discrete adjoints.

2. Case summary

Runs were performed using the ALE capability of the code, with a fourth order diagonally-implicit Runge-Kutta time stepping scheme. At each stage, the nonlinear system was solved using implicit Newton preconditioned with a line-Jacobi smoother. An impulsive free-stream velocity was set throughout the domain for the initial condition. However, the motions of the cylinder and airfoil were not imposed impulsively, but rather ramped-up over a time interval equal to approximately 3/4 of the first stroke period.

At each stage of the time stepping scheme, the residual was converged to an absolute L_1 norm below 10^{-8} using a conservative state vector with unit density and velocity, and gas constant $R = 0.4$. The Mach number was set to 0.2, while the Reynolds number and Strouhal number based on airfoil chord were set to 1000 and 0.2, respectively. Full-state boundary conditions were imposed on the farfield, and no-slip adiabatic wall boundary conditions were imposed on the cylinder and airfoil.

Initial runs were performed on the *nyx* supercomputing cluster at the University of Michigan, while final runs were performed on NASA's *Pleiades* cluster. On one core of *Pleiades*, one TauBench unit is equivalent to about 7.7 seconds of compute time, and final runs were performed on 800 cores each.

3. Meshes

The farfield boundary is a 26 x 26 chord-length square centered at the leading edge of the airfoil. Triangular meshes of approximately $25,000$ elements were used, with higher grid density close to the airfoil/cylinder. A close-up view of one of the meshes is shown below.

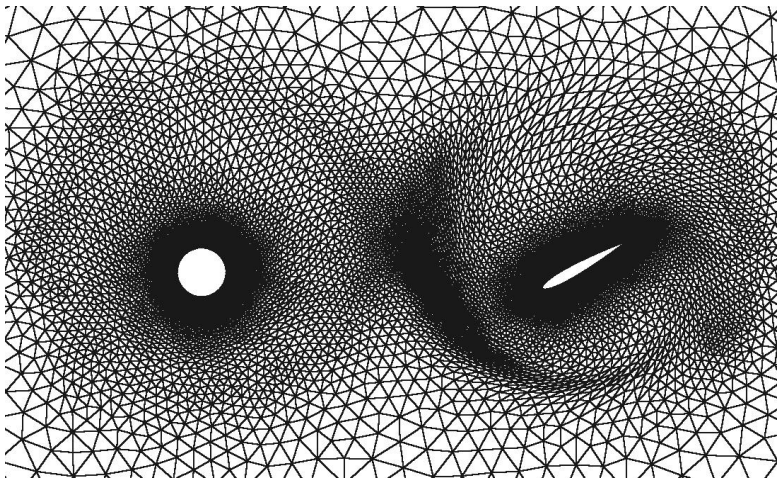

An arbitrary Lagrangian-Eulerian formulation was employed with motion as specified in the problem description. Grid deformation was specified analytically using blending functions of fifth order, at radii that were the maximum allowed by the proximity of the cylinder to the airfoil.

4. Results

The figures and tables below present the requested results for this case. Convergence studies were performed for both $s = 3.5$ and $s = 3.76$ cases. For these studies, the spatial resolution of each mesh remained fixed, while the solution interpolation order p and the number of DIRK4 time-steps was refined. Four refinements were performed, ranging from $p = 1$ with 900 time-steps to $p = 4$ with $4,200$ time-steps. Below, we show the results from our final $p = 4$ runs.

Solution Contours

In Figure 1, sample vorticity contours for both cases are shown, while sample entropy contours are shown in Figure 2.

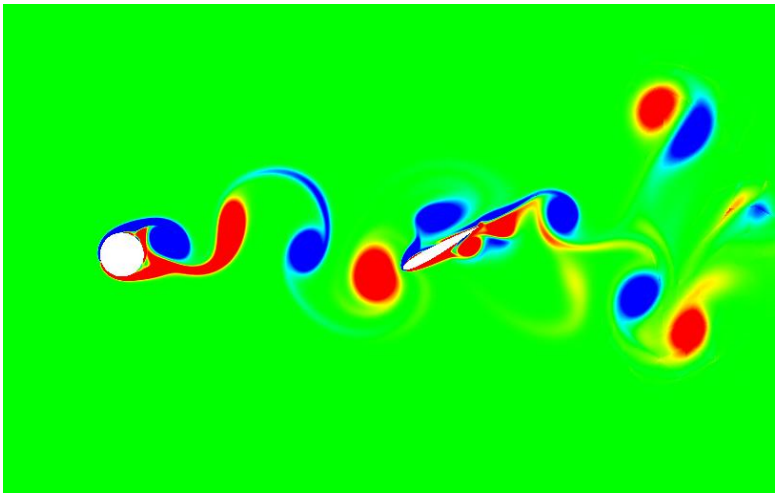

(a) $s = 3.5$

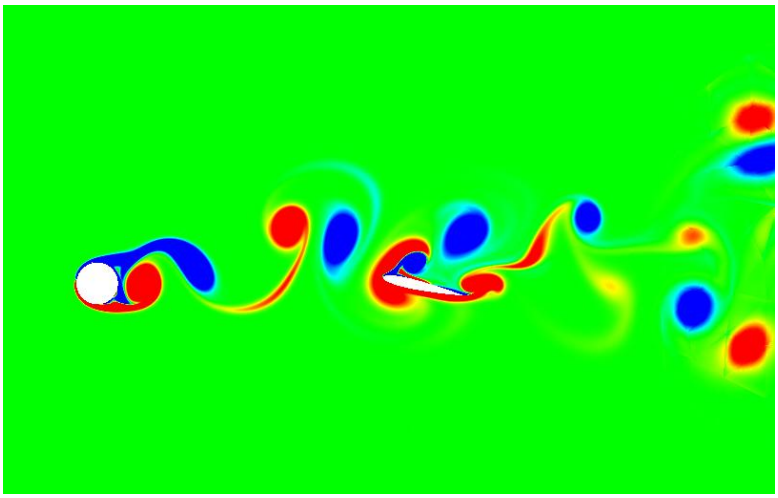

(b) $s = 3.76$

Figure 1: Vorticity contours at various points in the simulation for both cases.

From the solution contours, we see that the vortices shed from the cylinder interact with the airfoil downstream, which in turn sheds more vorticity into the wake. This vortex shedding is chaotic in nature, and causes a complicated wake structure to form in the far-field. It's this chaotic shedding

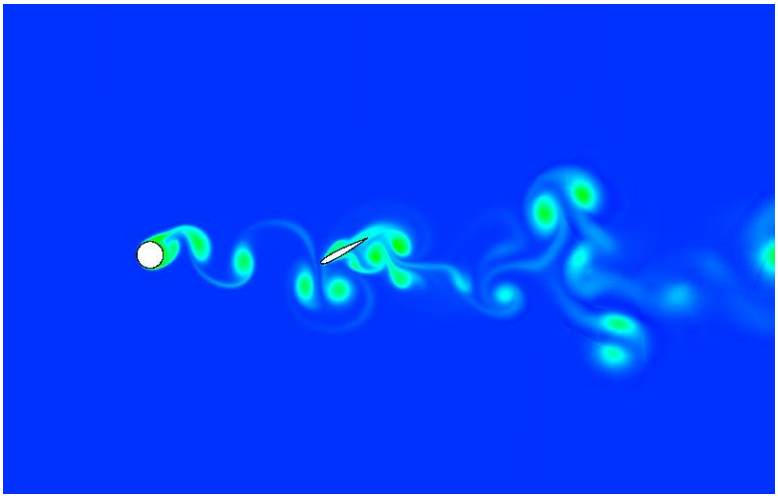

(a) $s = 3.5$

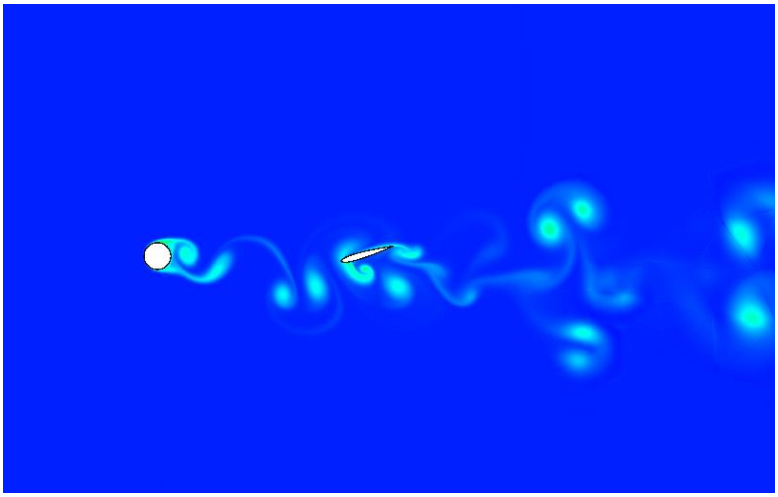

(b) $s = 3.76$

Figure 2: Entropy contours at various points in the simulation for both cases.

that keeps the flow from ever reaching a pseudo-steady state, as seen in the force histories presented in the following section.

Force Histories

Below, we present the force coefficient histories on the cylinder and airfoil for both cases. We see that modes with a lower frequency than the driving motion (which has a period of 5 time units) appear in the force histories, and that one of the main differences between the $s = 3.5$ and $s = 3.76$ cases seems to be a phase shift in the behavior of these lower-frequency modes. In addition, while the cylinder coefficients reach a nearly-pseudo-steady state, the chaotic vortex interactions near the airfoil keep it from ever reaching a similar state.

The fact that the forces are not pseudo-steady has implications when comparing results between groups, since it means that the details of the force histories will differ depending on the specific initial conditions used. In order to get a meaningful output for comparison, one option is to look at a long-

time average of the coefficients. In the following section, we show the convergence of these long-time averages as our meshes are refined.

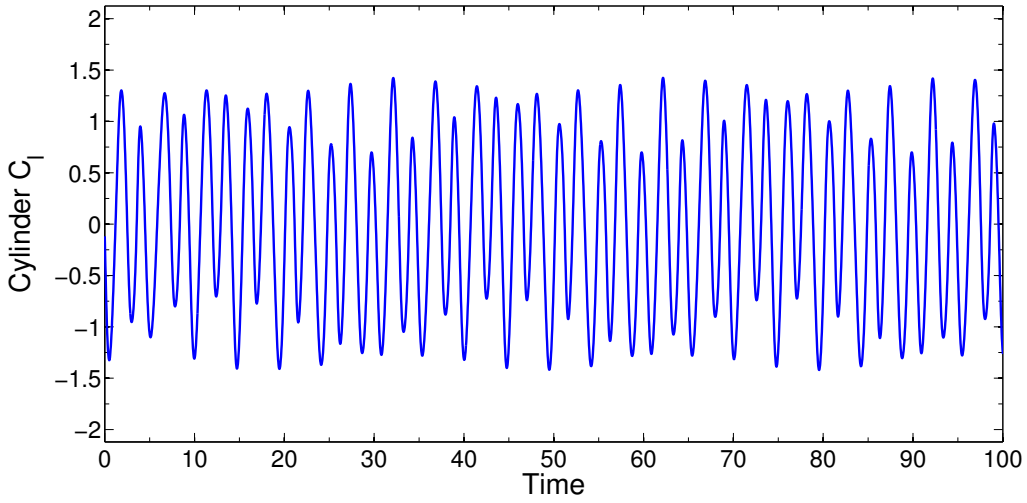

(a) $s = 3.5$

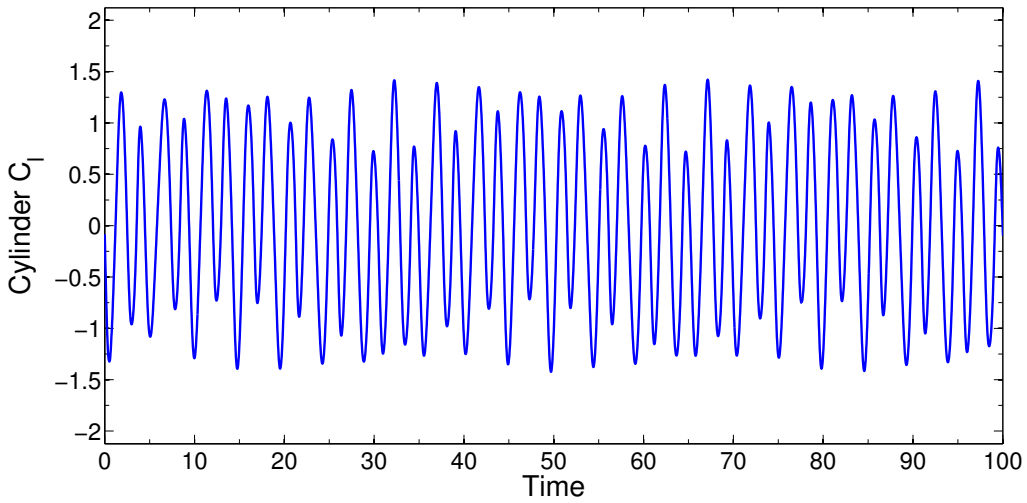

(b) $s = 3.76$

Figure 3: Time histories of the cylinder lift coefficient for both cases.

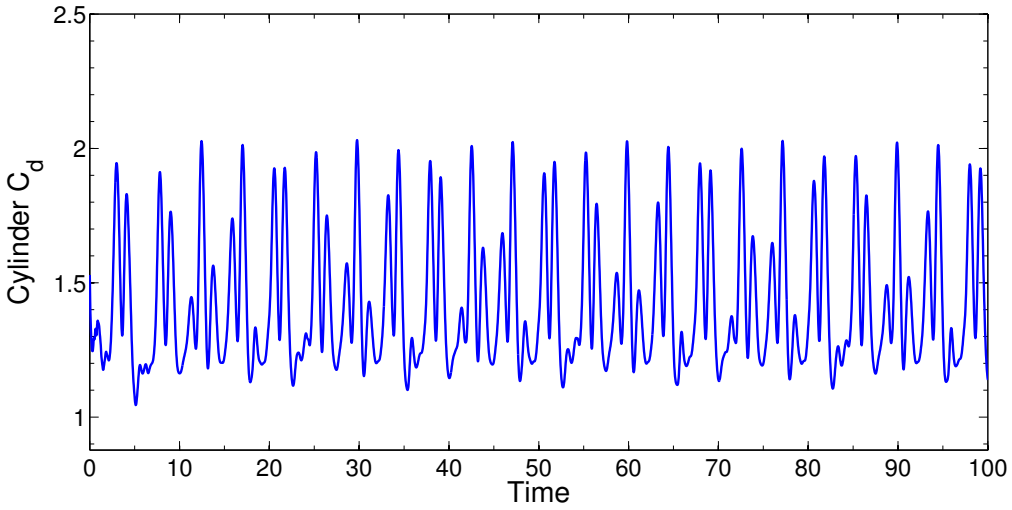

(a) $s = 3.5$

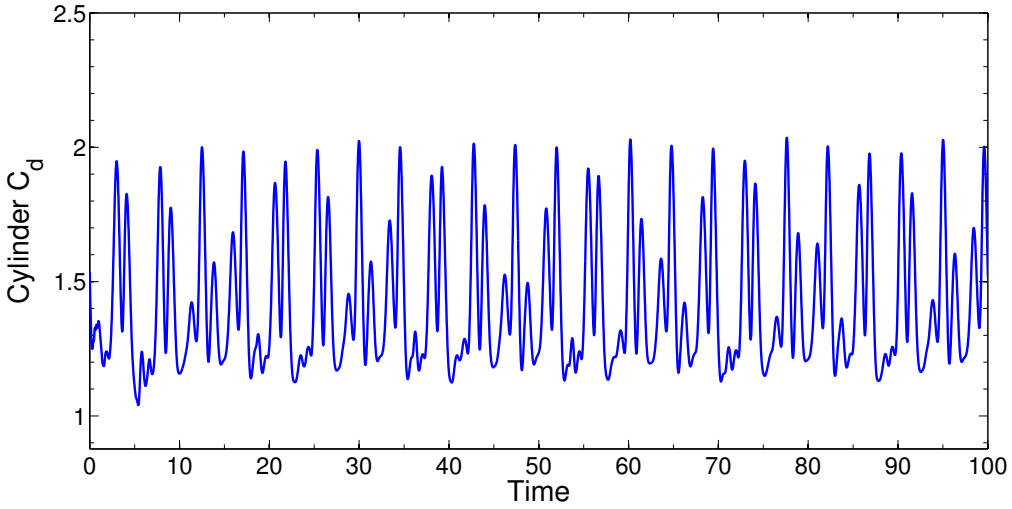

(b) $s = 3.76$

Figure 4: Time histories of the cylinder drag coefficient for both cases.

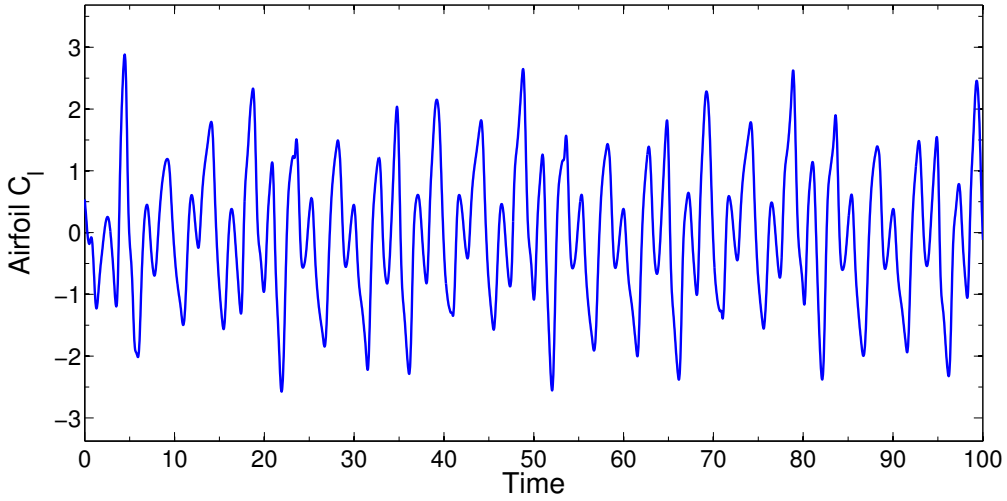

(a) $s = 3.5$

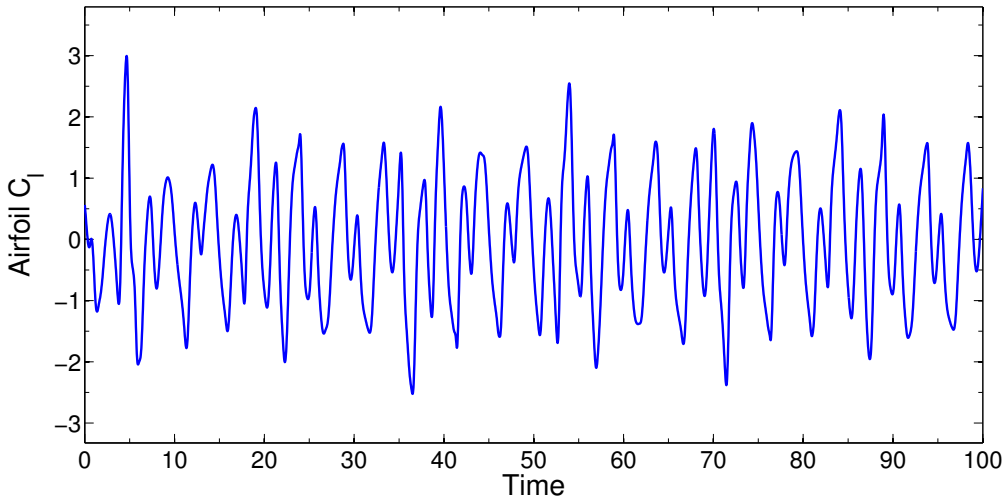

(b) $s = 3.76$

Figure 5: Time histories of the airfoil lift coefficient for both cases.

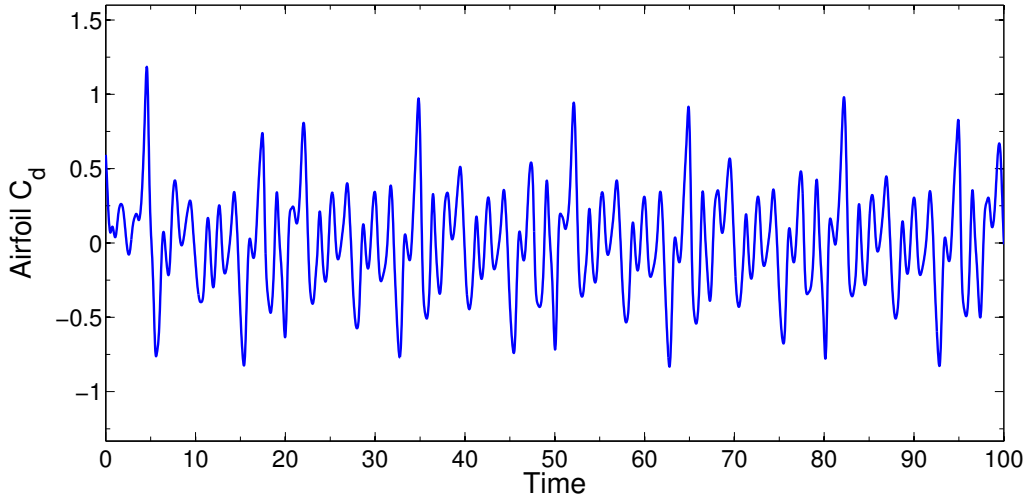

(a) $s = 3.5$

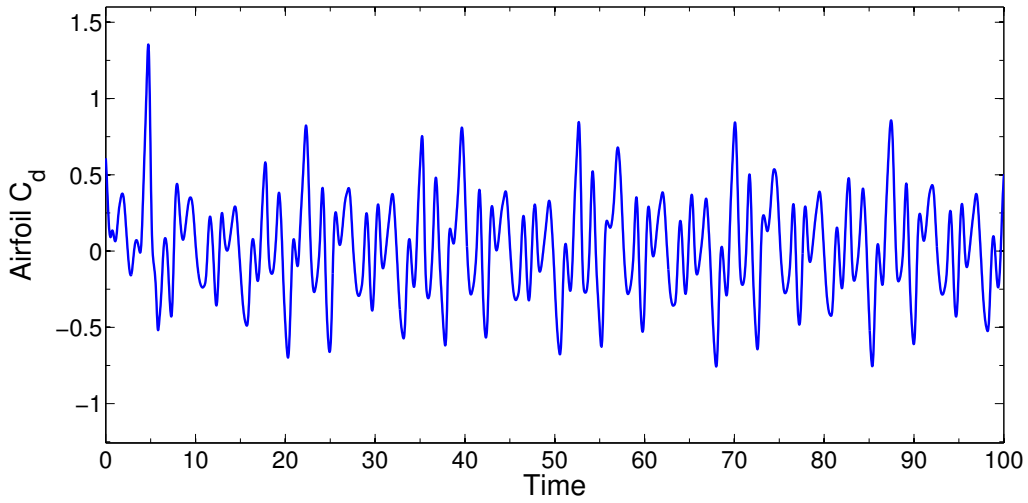

(b) $s = 3.76$

Figure 6: Time histories of the airfoil drag coefficient for both cases.

Convergence Studies

In this section, we present results showing both qualitative and quantitative convergence of the force coefficients. As mentioned, for our refinement studies we use a mesh with a fixed number of elements (approx. $25,000$) and refine both p and the number of timesteps to obtain a converged solution. The first three refinements, starting from a coarse mesh of $p = 1$ and 900 time-steps, were performed by uniformly incrementing p and doubling the number of timesteps. For the fourth refinement, we did not double the number of time-steps, but rather solved at $p = 4$ and $4,200$ time-steps.

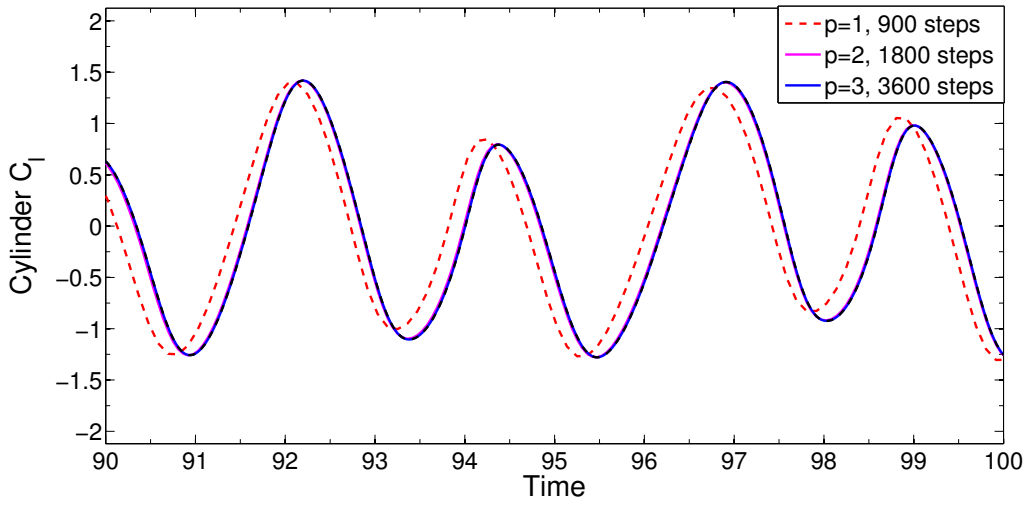

(a) Cylinder Cl, $s = 3.5$

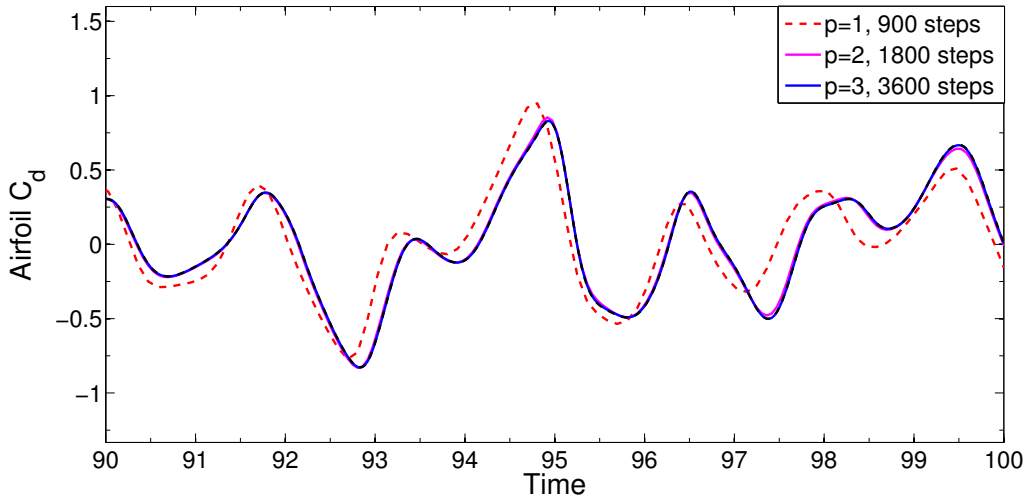

(b) Airfoil Cd, $s = 3.5$

Figure 7: Convergence of selected coefficients for the $s = 3.5$ case.

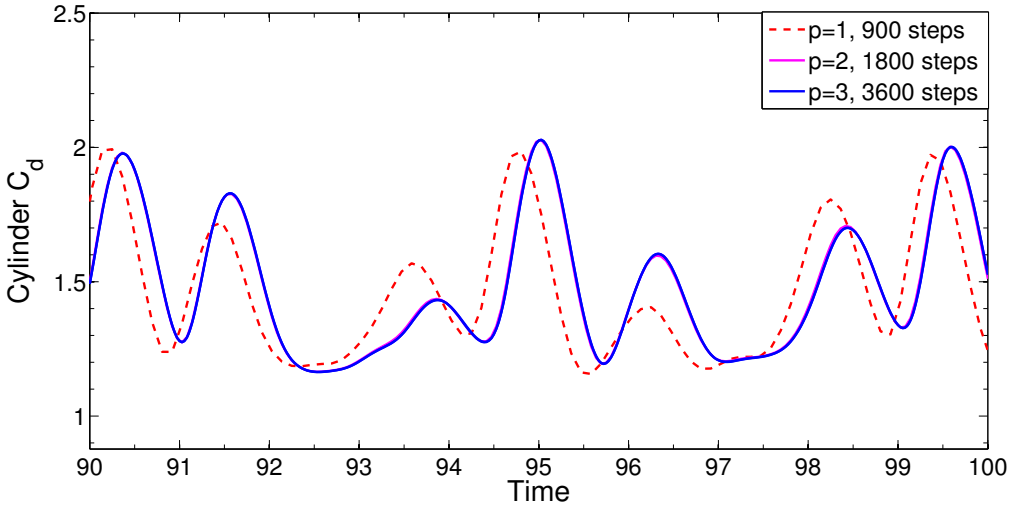

(a) Cylinder Cd, $s = 3.76$

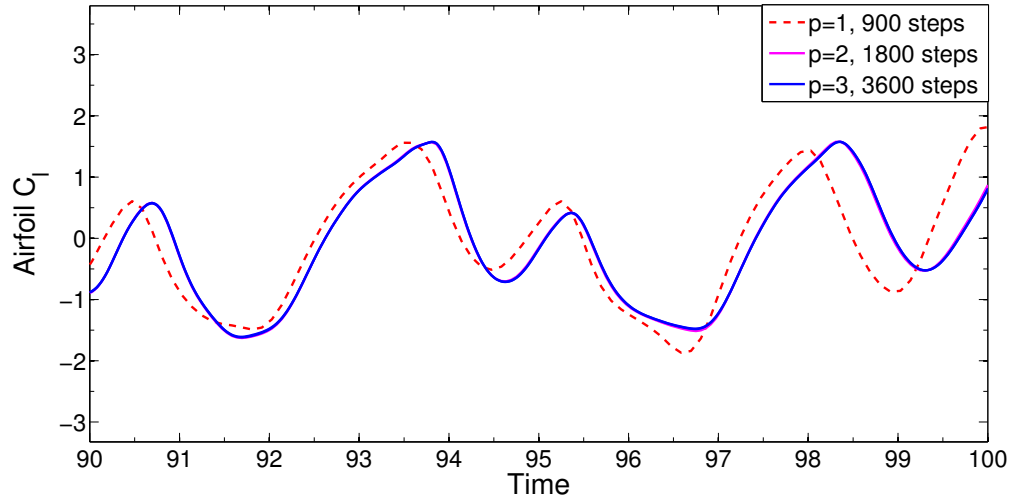

(b) Airfoil Cl, $s = 3.76$

Figure 8: Convergence of selected coefficients for the $s = 3.76$ case.

Figures 7 and 8 show the convergence of various coefficients over the last two periods of motion. As can be seen, the coarsest run deviates signficantly from the finer runs, but by $p = 3$ with $3,600$ timesteps the solution is visually converged. More quantitatively, we plot the convergence of the coefficient averages from $t = 20$ to $t = 100$ in Figures 9 and 10. From these figures, we see that all cylinder coefficients have converged to within 1 drag count by the final run. The airfoil coefficients are slower to converge, as expected, but are within an acceptable tolerance by the final run. The convergence of the airfoil lift coefficient in the $s = 3.76$ case is somewhat erratic, but this is likely due to the inherent difficulty of showing convergence for a value that should be zero by symmetry (averaged over a suitably long time).

Finally, these average force coefficients are given explicitly in Tables 1 and 2 below, along with the mesh information and TauBench work units.

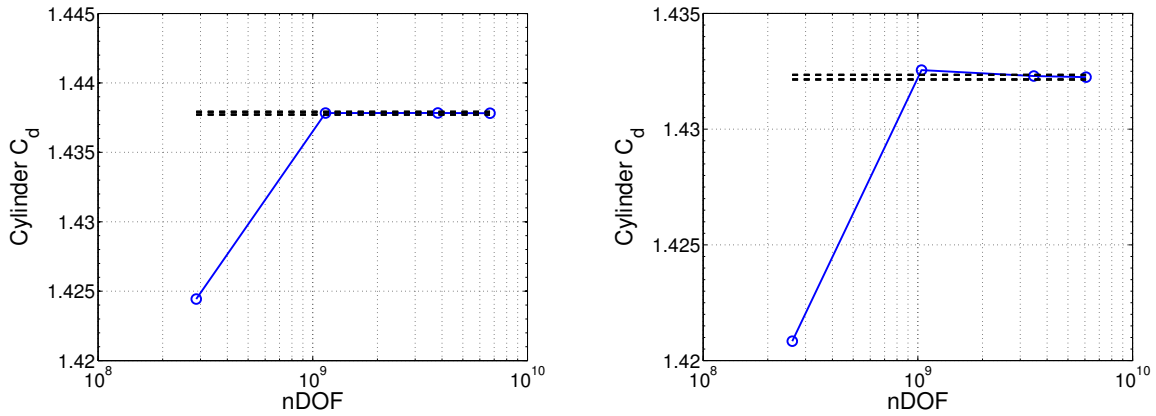

(a) $s = 3.5$

(b) $s = 3.76$

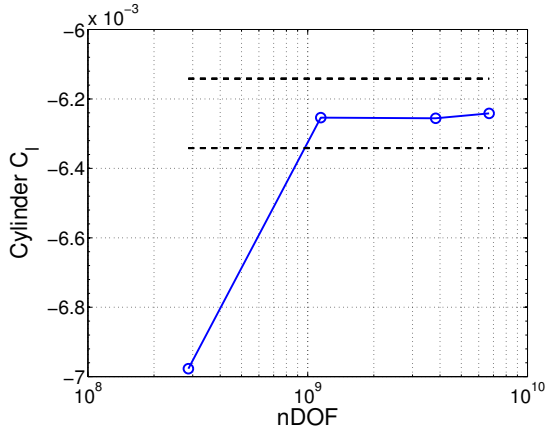

(c) $s = 3.5$

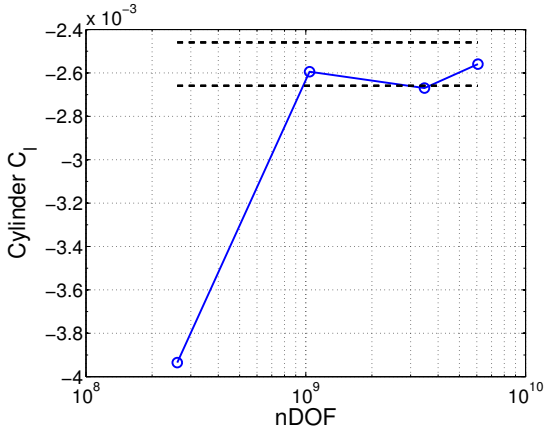

(d) $s = 3.76$

Figure 9: Convergence of average cylinder coefficients from $t = 20$ to $t = 100$. (Dashed black lines show ± 1 drag count from final value.)

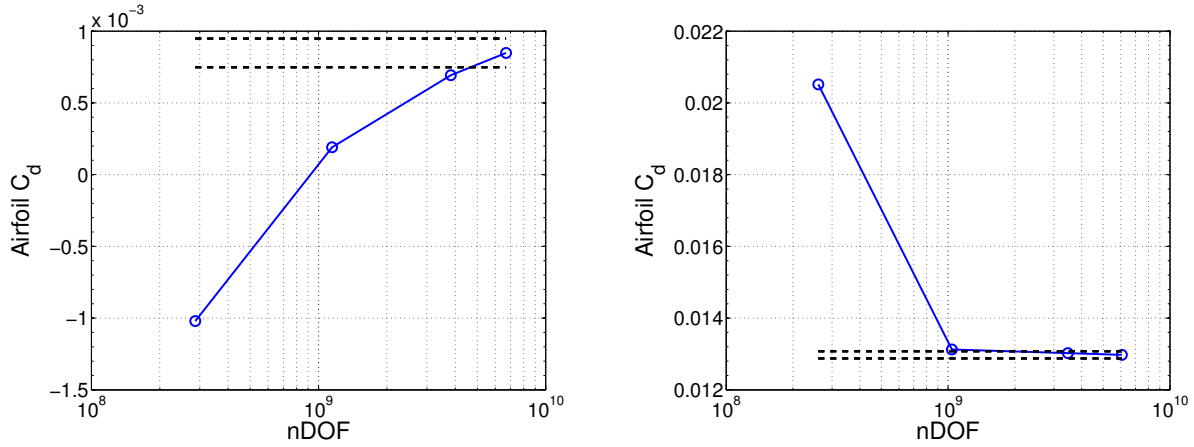

(a) $s = 3.5$ (b) $s = 3.76$

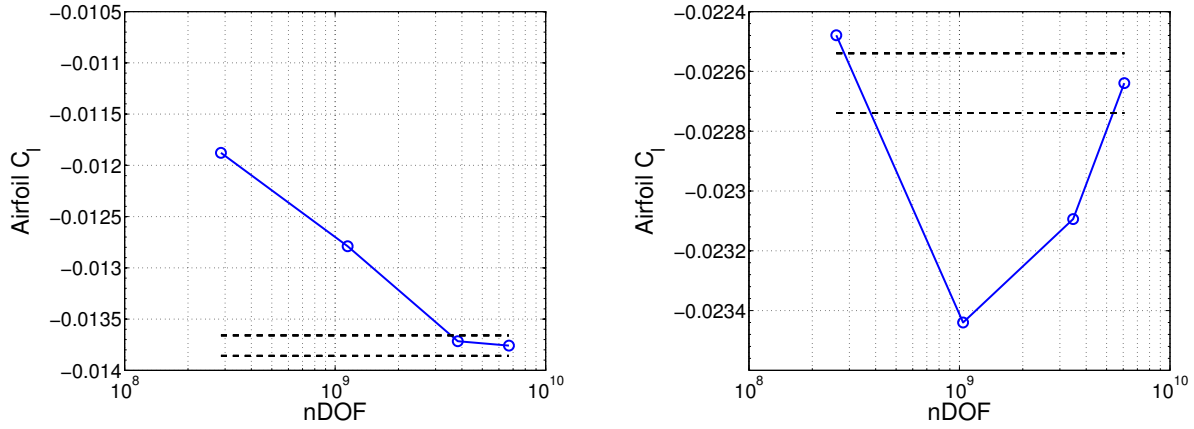

(c) $s = 3.5$ (d) $s = 3.76$

Figure 10: Convergence of average lift coefficients from $t = 20$ to $t = 100$. (Dashed black lines show ± 1 drag count from final value.)

Order	p=1	p=2	p=3	p=4
Timesteps	900	1800	3600	4200
TauBench	356,112.48	1,533,956.36	8,805,522.27	26,963,167.49
Airfoil Cd	-0.001020451225562	0.000190580136103	0.000692509959049	0.000848137761579
Airfoil Cl	-0.011877736328231	-0.012789438410407	-0.013715871110344	-0.013758723927219
Cylinder Cd	1.424435373267609	1.437831212463459	1.437836682821673	1.437820378959314
Cylinder Cl	-0.006977027451935	-0.006253903730250	-0.006255674063897	-0.006241543267989

Table 1: Output values with mesh refinement for $s = 3.5$ case.

Order	p=1	p=2	p=3	p=4
Timesteps	900	1800	3600	4200
TauBench	369,501.57	1,293,187.88	7,276,790.83	23,853,503.52
Airfoil Cd	0.020513600853644	0.013124788273664	0.013023922284510	0.012975272404322
Airfoil Cl	-0.022479002860897	-0.023439919163987	-0.023094151671026	-0.022639204487361
Cylinder Cd	1.420839739671724	1.432554954419297	1.432298106309817	1.432248885726691
Cylinder Cl	-0.003935323977657	-0.002594587085929	-0.002669907091131	-0.002559204389682

Table 2: Output values with mesh refinement for $s = 3.76$ case.